AGU PUBLICATIONS

JGR

Journal of Geophysical Research: Space Physics

RESEARCH ARTICLE
10.1002/2015JA021302

Global features of the disturbance winds during storm time deduced from CHAMP observations

Chao Xiong[1,2], Hermann Lühr[1], and Bela G. Fejer[3]

[1]GFZ German Research Centre for Geosciences, Potsdam, Germany, [2]Department of Space Physics, College of Electronic Information, Wuhan University, Wuhan, China, [3]Center for Atmospheric and Space Science, Utah State University, Logan, Utah, USA

Key Points:
- Disturbance zonal wind at subauroral region is related to SAPS
- Disturbance zonal wind peak at different MLTs for different latitudes
- Disturbance zonal wind needs 3–4 h from the auroral region to reach the equator

Correspondence to:
C. Xiong,
bear@gfz-potsdam.de

Citation:
Xiong, C., H. Lühr, and B.G. Fejer (2015), Global features of the disturbance winds during storm time deduced from CHAMP observations, *J. Geophys. Res. Space Physics*, *120*, 5137–5150, doi:10.1002/2015JA021302.

Received 2 APR 2015
Accepted 21 MAY 2015
Accepted article online 29 MAY 2015
Published online 22 JUN 2015

Abstract A wind-driven disturbance dynamo has been postulated many decades ago. But due to the sparseness of thermospheric wind measurements, details of the phenomena could not be investigated. In this study we use the CHAMP zonal wind observations from 2001 to 2005 to investigate the global features of the disturbance winds during magnetically disturbed periods. The disturbance zonal wind is mainly westward, which increases with magnetic activity and latitude. At subauroral region, the westward zonal wind is strongly enhanced in the magnetic local time (MLT) sector from afternoon to midnight, which we relate to the plasma drift within the subauroral polarization streams. At middle and low latitudes, the disturbance zonal wind is largely independent of season. Peak values of the disturbance zonal wind occur at different MLTs for different latitudes. That is around 1800 MLT at subauroal region, with average values of about 200 m/s; around 2300 MLT at middle latitudes, with average values of about 80 m/s; and around 0300 MLT at low latitudes, with average values up to 50 m/s. The shift of the peak values of the westward disturbance zonal wind in local time at different latitudes could be considered as a response of the disturbance wind when it propagates from high to low latitudes. Further by applying for the first time a superposed epoch analysis, we show that the disturbance zonal wind responds with a delay to the sudden changes of solar wind input, which is different for the various latitudinal ranges. The propagation time of disturbance wind from the auroral region to the equator is about 3–4 h. This is consistent with the speed of traveling atmospheric disturbances. Based on CHAMP observations, we try to illustrate the whole chain of processes from the solar wind driving to the ionospheric effects at lower latitudes.

1. Introduction

Thermospheric neutral winds are an important component in the coupled thermosphere-ionosphere system. In particular, at high latitudes the motion of neutral particles is controlled by both electrodynamic and hydrodynamic processes. Therefore, an understanding of the climatology of the neutral winds at quiet time as well as their response to geospace storms is necessary for predicting the dynamics of plasma and other constituents. During the past decades, extensive studies of winds have been carried out by Fabry-Perot interferometers (FPI) [e.g., *Rees et al.*, 1980; *Sipler et al.*, 1982; *Killeen et al.*, 1986; *Fejer et al.*, 2002, and references therein] and by incoherent scatter radars [e.g., *Sipler et al.*, 1991; *Aruliah et al.*, 1996; *Witasse et al.*, 1998; *Buonsanto and Witasse*, 1999, and reference therein]. Satellite missions have also been used for deriving wind observations, such as Dynamics Explorer 2 (DE 2) [*Thayer et al.*, 1987; *Killeen and Roble*, 1988], the Wind Imaging Interferometer (WINDII) aboard the Upper Atmosphere Research Satellite (UARS) [*Fejer et al.*, 2000; *Emmert et al.*, 2001, 2004], and, more recently, the CHAllenging Minisatellite Payload (CHAMP) mission [e.g., *Liu et al.*, 2006; *Lühr et al.*, 2007; *Doornbos et al.*, 2010; *Ritter et al.*, 2010]. These ground-based and in situ measurements, together with numerical and empirical models [*Richmond et al.*, 1992; *Hedin et al.*, 1996; *Ridley et al.*, 2006; *Codrescu et al.*, 2008; *Drob et al.*, 2008; *Emmert et al.*, 2008], have been used for investigating the diurnal, seasonal, and solar cycle variations of the thermospheric winds during both quiet and disturbed periods.

Thermospheric winds are mainly driven by the day-night difference in solar heating, by upward propagating atmospheric tides, by collisional interaction with rapidly convecting ions in the presence of strong electric fields, and by Joule heating associated with strong high-latitude electric currents [*Richmond et al.*, 2003b]. During quiet time the first two sources control the global wind pattern, while the latter two sources are highly variable and depend on the level of geomagnetic activity. They can produce thermospheric disturbance

winds, which will further affect the global ionospheric dynamo. In fact, at least two generalized source mechanisms exist for the disturbance electric fields and currents at middle and low latitudes. One is the prompt penetration electric field. Dynamic interactions between the solar wind and the magnetosphere cause electric currents following along the magnetospheric field lines. Some of these currents cause electric field, which penetrate directly to lower latitudes within the duct between Earth and ionosphere [e.g., *Kikuchi et al.*, 1996]. The second mechanism is the ionospheric disturbance dynamo. Energy input into the thermosphere during magnetic activity alters the circulation and consequently changes the generation of electric fields and currents at middle and low latitudes by ionospheric wind dynamo action [*Blanc and Richmond*, 1980]. We will address mainly the second mechanism within this study.

During magnetically active periods the thermospheric winds at middle and low latitudes have been frequently observed to differ from their quiet-day patterns. Based on observations from the Millstone Hill radar, *Babcock and Evans* [1979] reported stronger equatorward winds at nighttime during disturbed days, and *Buonsanto and Witasse* [1999] also reported significant magnetic activity effects on the meridional wind during solar minimum summer conditions. The daytime *F* region disturbance winds derived from WINDII at middle and low latitudes have been reported by *Fejer et al.* [2000] and *Emmert et al.* [2001]. Their results showed that disturbance winds increase roughly linearly with *Kp* and expand to lower latitudes with increasing magnetic activity. The zonal disturbance wind was largely independent of season, while the meridional disturbance wind was largest for low solar flux conditions. The different seasonal and solar flux dependences of disturbance zonal and meridional winds have been further confirmed by *Fejer et al.* [2002], by analyzing the nighttime disturbance winds over Millstone Hill.

Compared to the seasonal and solar flux variation, the disturbance winds show a clear dependence on latitude and magnetic local time (MLT). *Fejer et al.* [2000] reported that the average disturbance winds change significantly from morning to afternoon. *Emmert et al.* [2001] revealed that the disturbance zonal wind is mostly westward (except in the early morning hours). It increases with latitude and has the largest values in the later afternoon. Further by taking all the 24 MLT hours wind data from WINDII observations, *Emmert et al.* [2004] showed that with increasing local times, the location of the peak westward disturbance wind shifts to lower latitudes. *Liu et al.* [2006] reported that at middle and low latitudes the daytime zonal wind at CHAMP altitude is found to be less variable than the nighttime wind; in particular, it responses less to geomagnetic activities. Substorm-related disturbance winds have been analyzed by *Ritter et al.* [2010]. Their results show that the enhancement of the westward wind has average amplitudes of about 20 m/s at the equator and about 50 m/s near middle latitudes around midnight.

With all the studies mentioned above, great progress has been made for understanding the characteristic of the disturbance winds. However, the global feature and temporal evolution of the disturbance winds in response to a discrete solar wind input still need further investigation. The triaxial accelerometer on board CHAMP has been providing wind readings from August 2000 to the end of the 10 year mission, with excellent coverage of seasons, local time, and latitude. These data provide us a great opportunity for investigating the thermospheric zonal wind during disturbed periods. Therefore, in this study we try to illustrate the whole chain of processes from the solar wind driving to the ionospheric effects at different latitudes. In section 2 we introduce the thermospheric wind data derived from the CHAMP satellite. Section 3 describes the seasonal and local time dependence of the disturbance zonal winds. The interpretation of the wind observations as well as comparison with earlier studies will be given in section 4.

2. Data and Analysis

The CHAMP satellite was launched on 15 July 2000 into a near-circular polar orbit (inclination: 87.3°) with an initial altitude of 456 km. By the end of the mission, 19 September 2010, the orbit had decayed to 250 km. The orbital period was about 93 min, thus circling the Earth more than 15 times per day. The orbital plane scanned all local times within 131 days.

The zonal wind data used in this study are deduced from the accelerometer measurements on board the CHAMP satellite. The Spatial Triaxial Accelerometer for Research accelerometer was provided by the Centre National d'Etudes Spatiales (CNES). It measures the nonconservative forces exerted on the satellite with a resolution of $<10^{-9}$ m/s^2 in along-track and cross-track directions [*Reigber et al.*, 2002]. The advantage of deriving wind estimates from accelerometer measurements is that the method is quite direct and requires

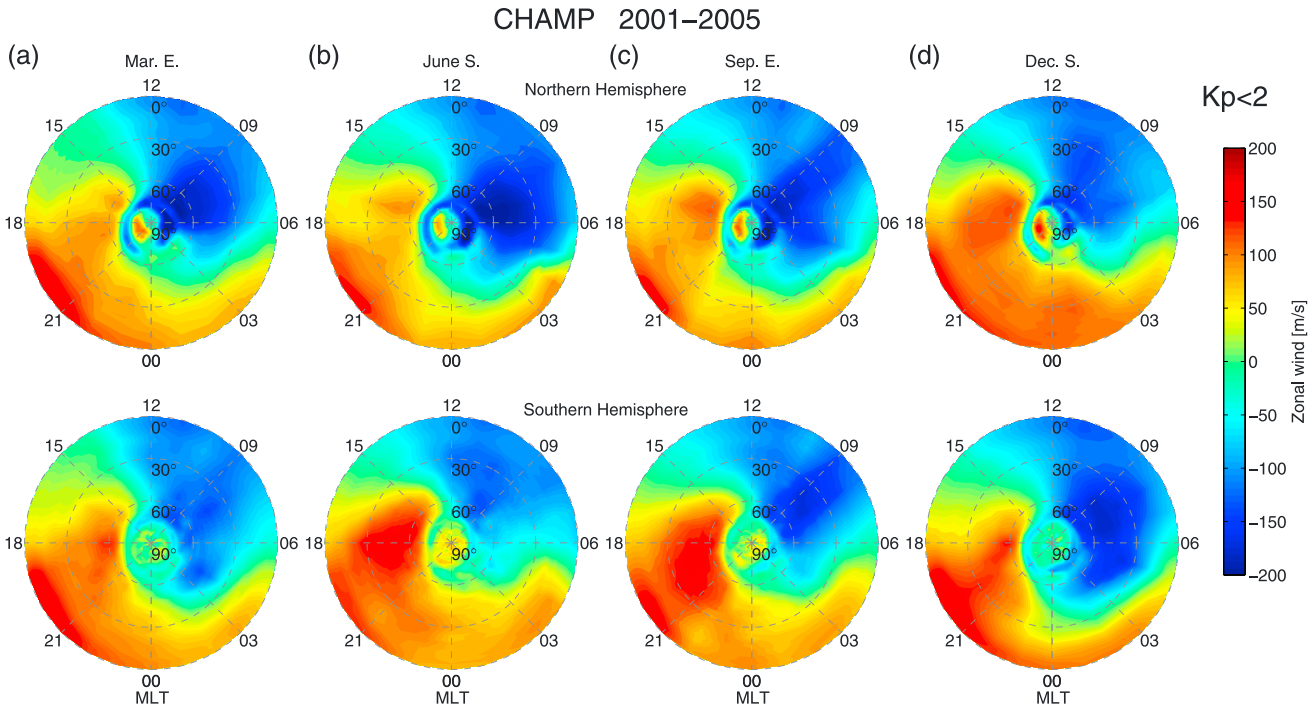

Figure 1. The magnetic latitude (MLAT) and local time (MLT) distribution of the average thermospheric zonal wind during magnetically quiet periods ($Kp < 2$) for (a) March equinox, (b) June solstice, (c) September equinox, and (d) December solstice seasons. Results from the Northern Hemisphere (top) and from the Southern Hemisphere (bottom). Positive velocities represent geographically eastward wind.

no special assumptions. For calibrating the accelerometer data several corrections were applied in order to isolate the forces caused by air drag. The calibration of the along-track accelerometer axis was performed by solving for daily accelerometer biases and comparing the readings with accelerations derived independently from GPS satellite-to-satellite tracking data [*VanHelleputte et al.*, 2009]. For the cross-track axis calibration an aerodynamic model of the satellite was applied to get more accurate results. In addition, extreme outliers, spacecraft attitude manoeuver effects, and accelerations due to solar radiation pressure were removed. The full details of the processing algorithm can be found in *Doornbos et al.* [2010].

With the approach described above, the accelerometer data of CHAMP (from May 2001 to December 2008) have been processed to obtain thermospheric mass density and zonal wind. Data were averaged over time intervals of 10 s, achieving a resolution of <10 m/s for the zonal wind [*Doornbos et al.*, 2010]. However, the wind signals at CHAMP altitude became too weak and unreliable during the recent solar minimum (2008–2009). For that reason the time period considered in this study is the higher and moderate solar activity years (2001–2005). The wind measurements have further been divided into four seasons, centered on March equinox, June solstice, September equinox, and December solstice. For each season overlapping periods of 131 days are needed to cover all 24 local time hours.

3. Results

The zonal wind measurements from CHAMP used in the following section are treated in magnetic quasi-dipole coordinates [*Richmond*, 1995; *Emmert et al.*, 2010] rather than in geographic coordinates, in order to highlight the thermospheric response to the plasma dynamics.

3.1. Climatology of Thermospheric Zonal Wind During Quiet and Magnetically Disturbed Periods

To give a global view of the average thermospheric zonal wind during magnetically quiet periods, data from times of $Kp < 2$ are used, as shown in Figure 1 (positive value refers to geographically eastward direction). We can see that at middle and low latitudes the quiet time zonal wind is generally directed eastward from post-noon to early morning and westward for the other local times. This typical diurnal variation at low latitudes is largely independent of season, while slight seasonal effects can be seen at middle latitudes during solstice seasons, with larger westward wind speed at nighttime in the summer hemispheres. In polar cap regions

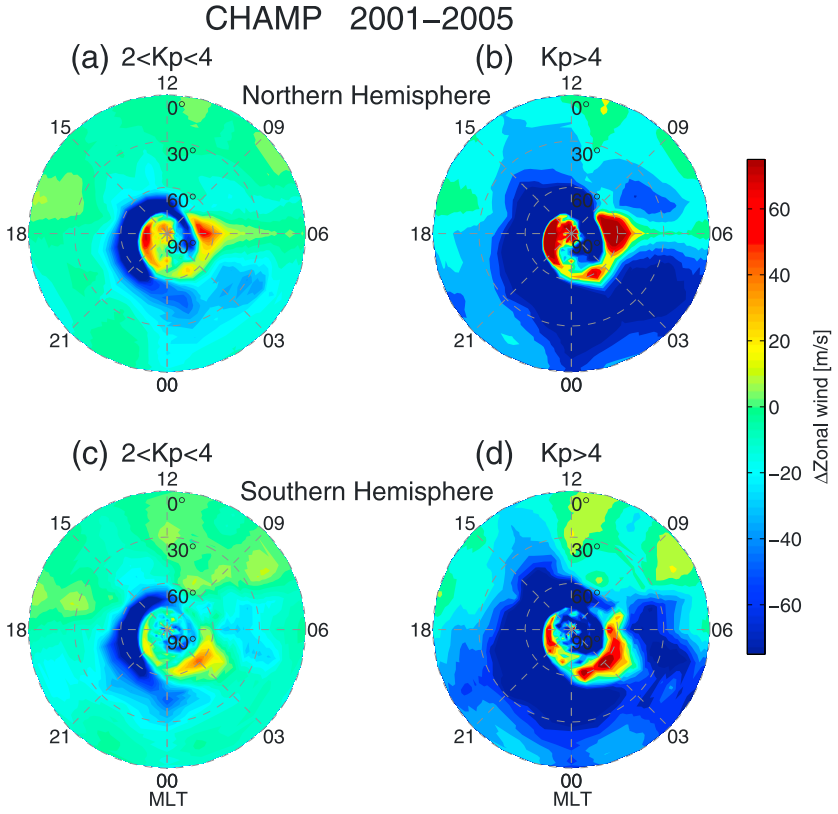

Figure 2. Same format as Figure 1 but for the disturbance zonal wind during moderate ($2 < Kp < 4$) and active ($Kp > 4$) magnetic disturbed periods. Data from all seasons are combined.

(beyond 70° magnetic latitude), CHAMP readings do not represent zonal winds anymore properly. Here the data require a different interpretation for resolving the wind pattern [e.g., *Lühr et al.*, 2007].

Next we will focus on the disturbed periods. The data have been sorted into two groups for moderate ($2 < Kp < 4$) and active ($Kp > 4$) magnetic disturbed periods. Figure 2 presents the magnetic latitude (MLAT) versus MLT distribution of the disturbance zonal wind (we subtracted the corresponding quiet time values) for different disturbed levels and separately for the two hemispheres. Data from all seasons have been combined. Generally, stronger westward disturbance wind is found with increasing magnetic activity. Under moderate disturbances ($2 < Kp < 4$) an eastward enhancement of zonal wind appears during morning hours at subauroral latitudes, while from noon to midnight a westward disturbance zonal wind dominates at subauroral and midlatitudes, extending to low latitudes past midnight. For more geomagnetically active periods ($Kp > 4$) strong westward disturbance zonal winds propagate equatorward with increasing MLT. Eastward perturbation winds are mainly confined to auroral and subauroral regions.

As already mentioned above, this study mainly focuses on the storm-driven disturbance winds. Therefore, we are more interested in the effects at latitudes from the subauroral to the equatorial regions. Data have been sorted into three regions, low latitudes (±20° MLAT), middle latitudes (±20° to ±50° MLAT), and subauroral (±50° to ±70° MLAT). The ±50° to ±70° MLAT range includes part of the auroral zone. However, the subauroral region is more important for the disturbance wind. Therefore, we refer to it within this study. First, we have to look at the general variability of thermospheric winds. Figure 3 presents the standard deviation of the average zonal wind diurnal variation as shown in Figures 4–6 separately for the three different latitude bands. CHAMP data for all seasons and activity levels are combined. It is worth to mention that the standard deviation presented here is not the error of zonal wind (the resolution of CHAMP zonal wind is less than 10 m/s [*Doornbos et al.*, 2010]) but mainly corresponds to physical variations. We can see that the zonal wind shows large variations, in particular, at high latitudes. The standard deviation is largest after nighttime and has a minimum during daytime at all latitude ranges. It implies that many other effects like tides influence the wind and the greater air density during daytime reduces the variability.

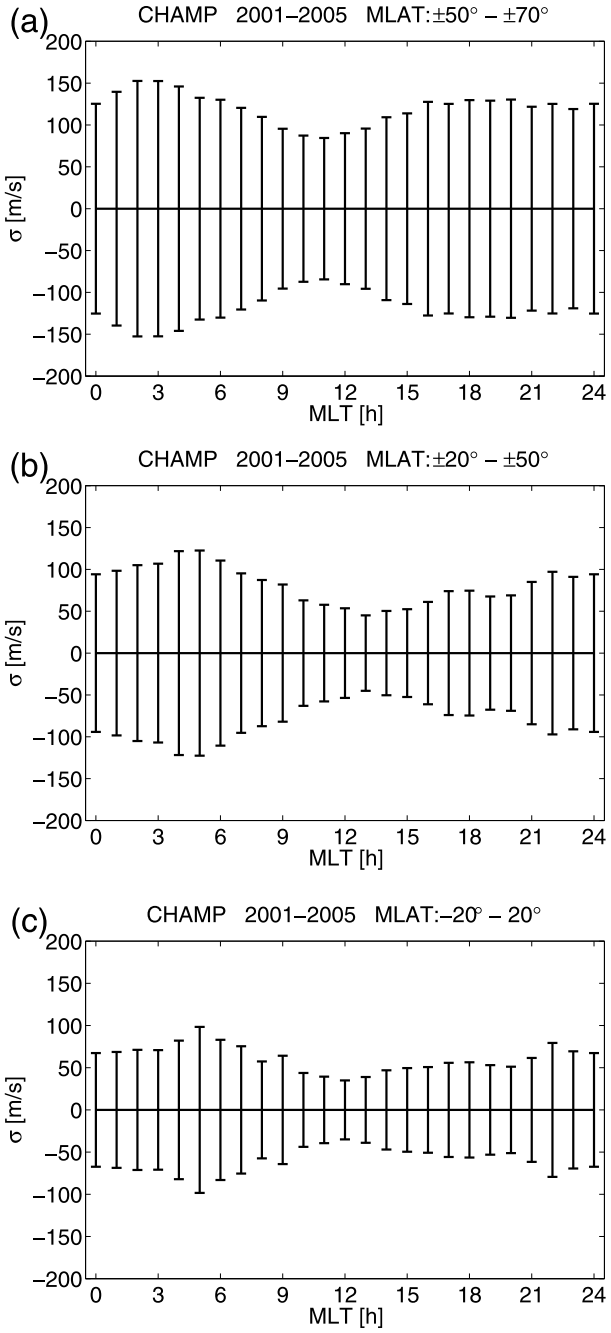

Figure 3. Local time variations of the standard deviation with respect to the zonal wind diurnal variation at different latitudes: (a) subauroral region, (b) middle latitudes, and (c) low-latitude region. Data from both hemispheres and all seasons, as well as from quiet and disturbed times, have been combined.

Of particular interest here is the systematic influence of magnetic disturbances on the thermospheric winds. Figures 4–6 present the longitudinally averaged diurnal variations of zonal wind during quiet time (top) and the perturbations during disturbed periods (bottom) for the three different latitude ranges. Data have been plotted separately for the four seasons and two hemispheres to check whether there are dependences of the perturbation winds. During quiet times the zonal wind exhibits a typical diurnal variation at all the latitude bands, blowing westward at daytime and changing sign to eastward around 1500 MLT at equatorial regions, with earlier reversal time for higher latitudes (around 1300/1400 MLT for subauroral/middle latitude regions). But the disturbance zonal winds show quite different diurnal variations at the three latitude bands. At the subauroral region (shown in Figure 4), we find almost no modification of the wind in the local time sector from midnight to 0900 MLT. After that strong westward disturbance zonal winds are found around sunset (from 1500 to 2000 MLT), with peak values of about 200 m/s, while at middle and low latitudes the time sector unaffected by magnetic activity is more centered on the daytime hours (0700–1700 MLT). As can be seen in Figure 5, large westward wind deflections appear around 2300 MLT, with peak values of about 80 m/s. Even later during postmidnight hours, the westward disturbance wind reaches equatorial regions with peak values of about 50 m/s (see Figure 6).

For moderately disturbed periods we observe rather similar diurnal variations as during active periods, but the amplitudes are smaller by at least a factor of 2, and peak disturbances tend to appear at later local times (e.g., Figure 4).

3.2. Superposed Epoch Analysis for the Disturbance Winds

As we want to obtain the temporal evolution of the disturbance wind, we applied a superposed epoch analysis to the CHAMP observations. We use a sudden increase in solar wind input as the key time. Time series of disturbance winds are stacked relative to the key time and then averaged. In case of satellite observations only snapshots of wind observations within a latitude range can contribute once per orbit. Therefore, a large number of events are required for obtaining statistically significant results.

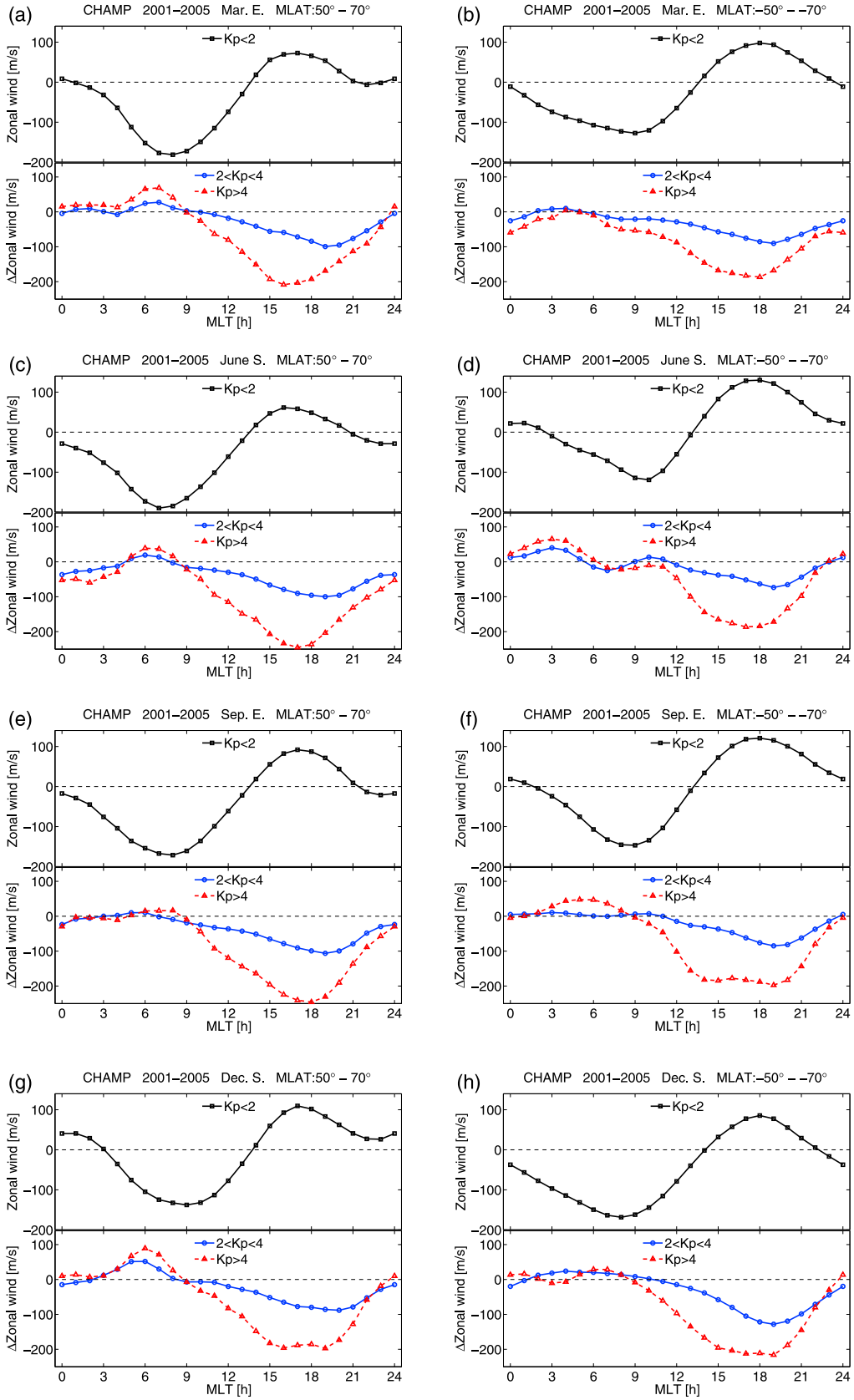

Figure 4. The longitudinally averaged (top) diurnal variations of the quiet time zonal wind, as well as (bottom) the wind perturbations during disturbed periods for the subauroral region (±50° to ±70° MLAT).

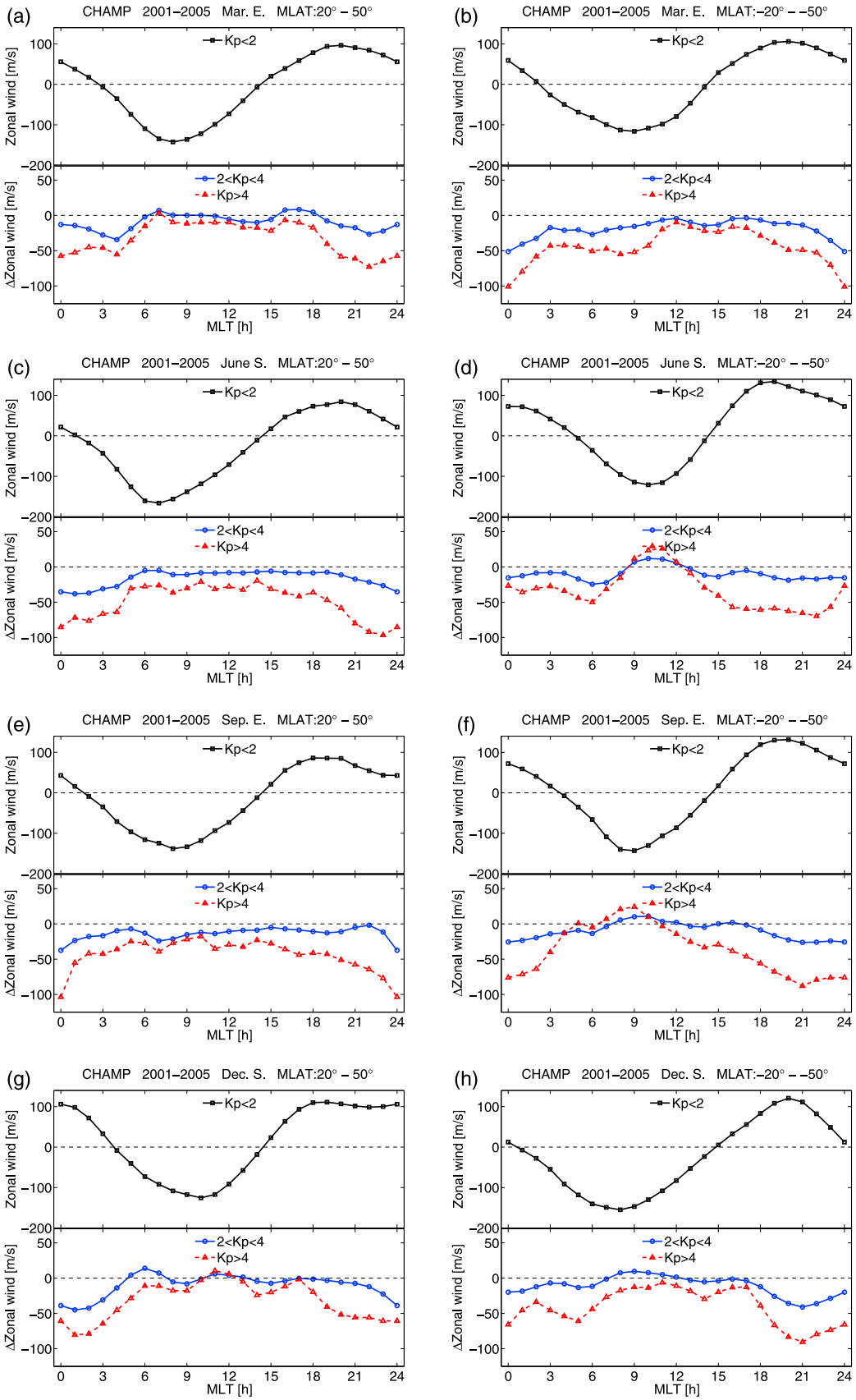

Figure 5. Same as Figure 4 but for the middle latitudes (±20° to ±50° MLAT).

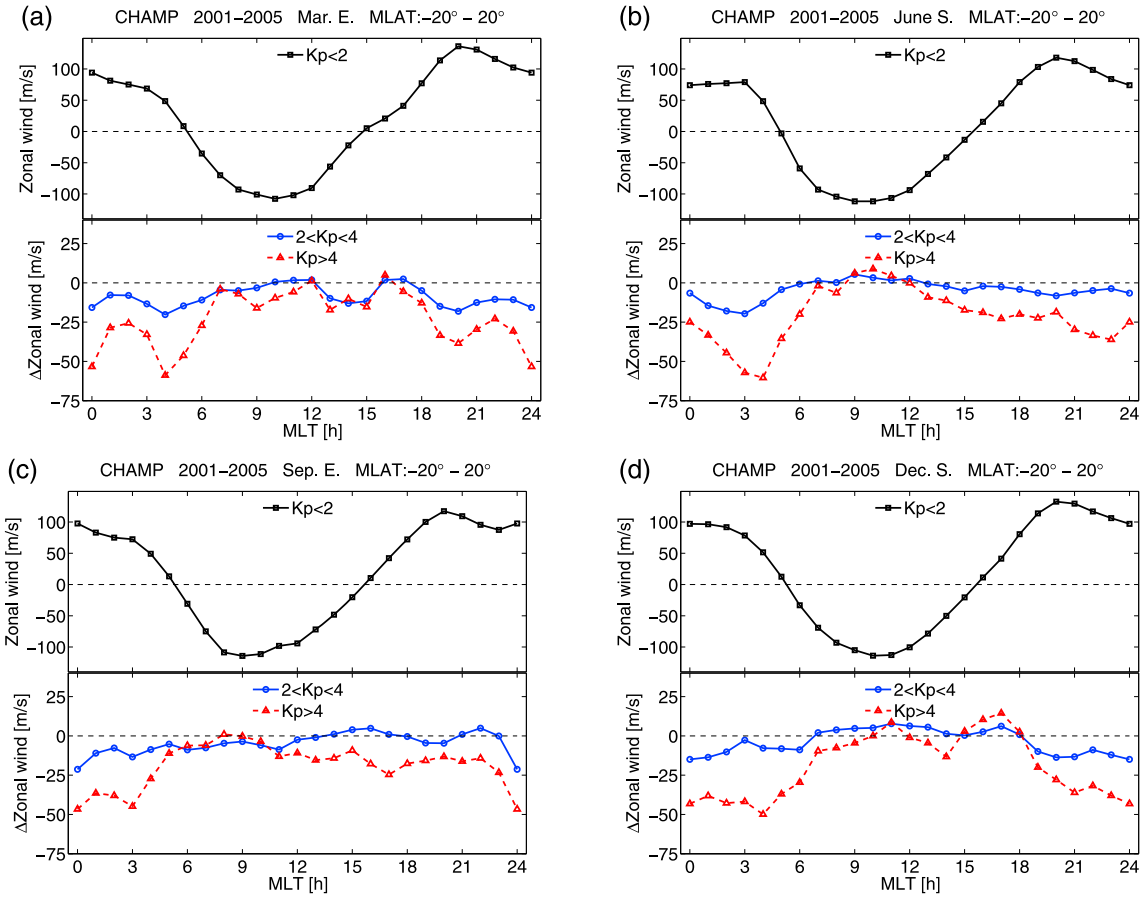

Figure 6. Same as Figure 4 but for the low-latitude region (±20° MLAT).

Burke et al. [2007] reported that the polar cap potential correlates fairly well with the thermospheric density changes during storms. However, the availability of polar cap potential measurements from DMSP is poor. Alternatively, *Liu et al.* [2010] used the merging electric field to predict the mass density changes related to storm effects. As the merging electric field is a physical quantity, which closely correlates with polar cap potential and can be easily obtained from solar wind and interplanetary magnetic field (IMF) data, we prefer to use this quantity for representing the solar wind energy input into the ionosphere-thermosphere system. The coupling function is as defined by *Newell et al.* [2007]:

$$E_m' = V_{sw}^{\frac{4}{3}} \left(\sqrt{B_y^2 + B_z^2} \right)^{\frac{2}{3}} \sin^{\frac{8}{3}}\left(\frac{\theta}{2}\right) \tag{1}$$

where V_{sw} denotes the solar wind velocity, B_y and B_z denote the y and z components of the IMF in geocentric solar magnetospheric coordinates, and θ is the clock angle of the IMF ($\tan(\theta) = \frac{|B_y|}{B_z}$). To make the numerical values comparable with the merging electric field (in mV/m) defined by *Kan and Lee* [1979], we use for calculating the E_m' in equation (1), V_{sw} in units of km/s, and B_y and B_z in nT and then divided the result by a factor of 3000.

Richmond et al. [2003a] pointed out that due to the inertia of the air, the changes of thermospheric wind lag behind the changes in the IMF. In their study densities were correlated with lagged and time-averaged IMF values. This kind of memory effect of the magnetosphere-ionosphere-thermosphere system with respect to solar wind input changes has also been used by previous studies [e.g., *Werner and Prölss*, 1997; *Liu et al.*, 2010]. From this point of view, we use the same procedure for deducing the effective merging electric values. The time-integrated merging electric field (E_m) can be defined as

$$E_m(t,\tau) = \frac{\int_{t_1}^{t} E_m'(t') e^{(t'-t)/\tau} dt'}{\int_{t_1}^{t} e^{(t'-t)/\tau} dt'} \tag{2}$$

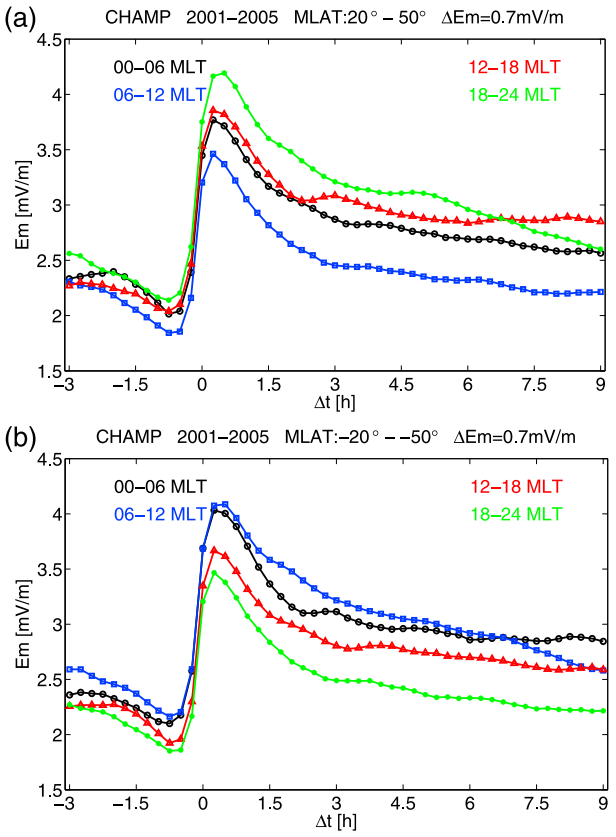

Figure 7. The temporal variation of the merging electric field (from 3 h before to 9 h after the key time) for the events when CHAMP is passing middle latitudes in the (a) Northern and (b) Southern Hemispheres.

where E_m' is treated as a continuous function of time t', t_1 is chosen 3 h before the actual epoch, and τ is the *e*-folding time of the weighting function in the integrands, with a value $\tau = 0.5$ h. A similar approach for calculating the merging electric field has been used in our previous studies [*Xiong et al.*, 2014; *Xiong and Lühr*, 2014].

From equations (1) and (2), we calculate the parameter E_m at time steps of 15 min. For the superposed epoch analysis we use a sudden increase of E_m as key time. The time step $t = n + 1$ is taken as key time for a magnetic disturbance if $E_m(n + 1) - E_m(n) > 0.7$ mV/m. The average evolution of the zonal disturbance wind with respect to the key time is deduced for different latitudes and local times. The data have been sorted again into subauroral (±50° to ±70° MLAT), middle latitude (±20° to ±50° MLAT), and equatorial regions (±20° MLAT). For each latitude bin, four local time sectors (0000–0600, 0600–1200, 1200–1800, and 1800–2400 MLT) have been selected.

First, we have to look at the average evolution of the merging electric field around the key time defined as $t = 0$. Figure 7 shows the temporal variation from 3 h before to 9 h after the key time for the events when CHAMP is passing middle latitudes. E_m variations are looking similar for the other latitude regions. Quite prominent is the sudden jump of E_m at the key time. We observe typically a peak-to-peak increase of 1.8 mV/m. This can be regarded as a significant change in solar wind input. For the southern hemispheric passes of CHAMP the E_m curves are rather similar as in the Northern Hemisphere. In both hemispheres local time sectors have been sampled at somewhat different solar wind activity levels resulting in slightly different levels of the various curves. It is worth noting that we find rather high levels of E_m (above 2 mV/m) already before the event time. The values drop slightly before the steep increase. After the peak E_m values decrease quite rapidly during the first 1.5 h, then only gradually for the later time.

The response of the disturbance wind to a step-like increase of solar wind input is shown in Figure 8. The time resolution has been chosen to be 1.5 h, which equals approximately the CHAMP orbital period. Starting at subauroral latitudes, as shown in Figures 8a and 8b, clearly different variations of disturbance zonal wind are observed within the four local time sectors. Overall, the early morning and prenoon sectors are less affected than the other two. The most prominent response is observed in the afternoon sector, as expected from Figure 4. Here westward disturbance winds are fairly strong already before the key time due to the substantial solar input before the events (see Figure 7). Right at the key time, westward winds get stronger and peak at 1.5 h (after one orbit). A similar evolution is observed in the premidnight sector but at a lower level. Furthermore, the peak disturbance winds are reached about 1.5 h later in that sector. The wind in the postmidnight (0000–0600 MLT) sector is on average only weakly affected by the solar wind input. But shortly after the key time, it exhibits a moderate eastward enhancement.

At middle latitude the disturbance wind is significantly weaker, as shown in Figures 8c and 8d. Here we observe the largest effects in the postmidnight sector. Strongest westward winds occur 3–4.5 h after the input time. The premidnight sector (1800–2400 MLT) shows again a similar albeit weaker response to the increased solar

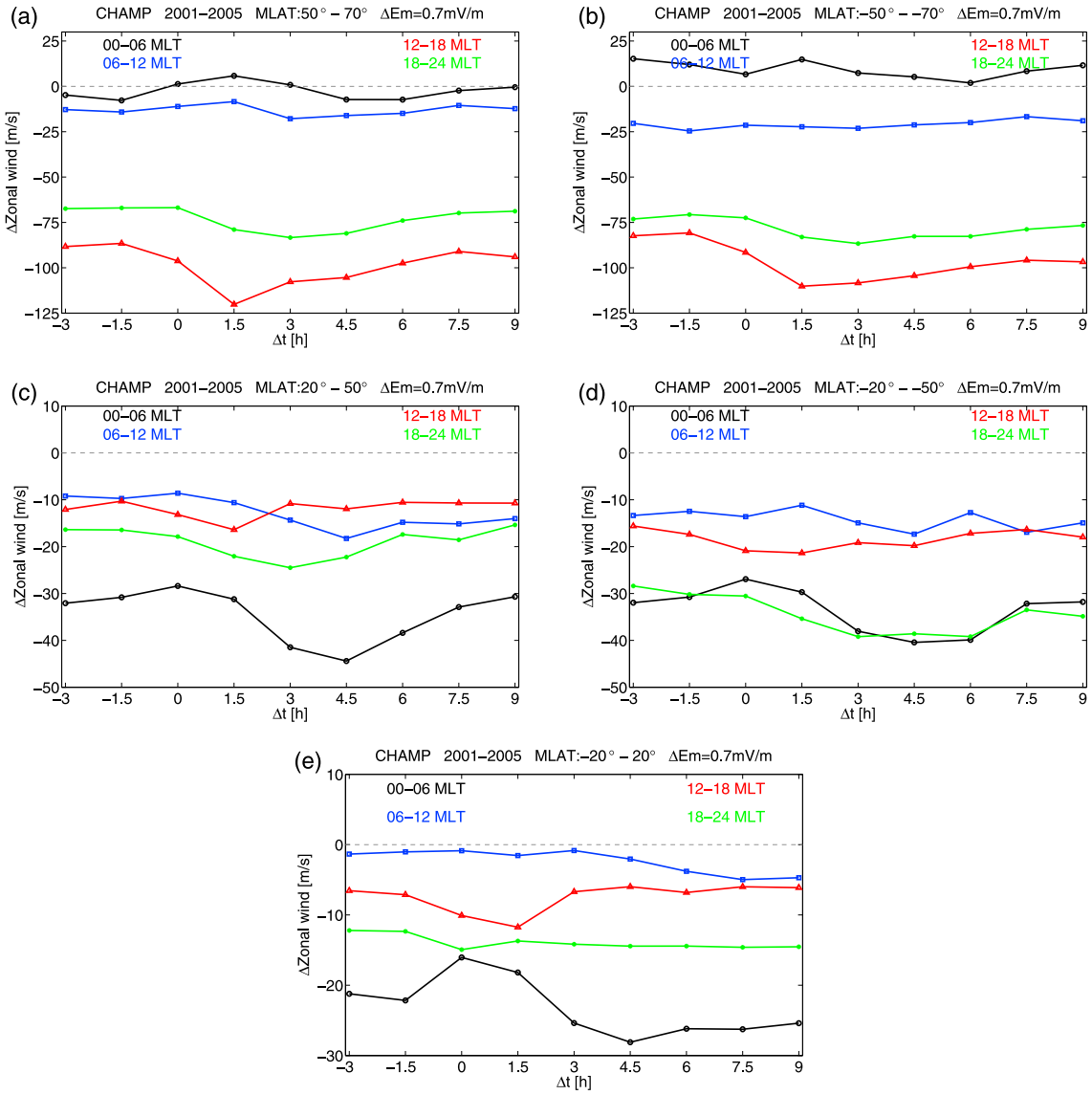

Figure 8. The temporal evolution of the disturbance zonal wind (from 3 h before to 9 h after the key time) for the events when CHAMP is passing (a and b) subauroral region, (c and d) middle latitudes, and (e) low-latitude regions.

wind input. In this sector peak westward winds are reached somewhat earlier than in the postmidnight sector. In the other two local time sectors the variations are fairly weak.

Finally, we have a look at the disturbance wind evolution at low latitude, as shown in Figure 8e. Again, the largest effects are observed in the postmidnight sector. At the time of the E_m step ($t = 0$) we find a short weakening of the westward wind. This is followed by an enhanced westward peaking at $t = 4.5$ h. The evolution of disturbance wind varies in the afternoon sector (1200–1800 MLT) in antiphase with that at 0000–0600 MLT albeit with smaller amplitudes. The immediate response at $t = 0$ we regard to be an effect of the prompt penetration electric field. It obviously adds a westward component during the afternoon and an eastward component after midnight to the *F* region zonal wind at low latitudes. The second largest westward disturbance winds are observed in the 1800–2400 MLT sector but with small evolutional variations. We find at low latitudes the smallest effects of the solar wind input on the wind during 0600–1200 MLT.

In summary of the superposed epoch analysis we may state that disturbance wind effects are observed first at subauroral latitudes and progressively later at lower latitudes. This suggests an equatorward propagation from high latitudes of both hemispheres. The time difference between peak effects at 60° MLAT and the equator amounts to about 3 h. This corresponds to a propagation speed of 610 m/s. On the other hand, the local

time of the peak effect changes from 1800 MLT at 60° MLAT to 0300 MLT at the equator. The average temporal evolution of the zonal disturbance wind after a step-like input is practically the same in both hemispheres. Attempts for interpreting these observations will be given in the next section.

4. Discussion

We have presented the global features of the thermospheric zonal winds at *F* region height during quiet and magnetically disturbed periods, based on 5 years of observation from the CHAMP satellite. In the subsequent section we are going to interpret and compare our results with previous studies.

4.1. Local Time and Latitudinal Variations of the Disturbance Zonal Wind

Disturbance winds at middle and low latitudes during daytime and nighttime have been separately reported by earlier studies. Based on observations from the WINDII instruments on the UARS satellite, *Fejer et al.* [2000] and *Emmert et al.* [2001] reported that the daytime disturbance zonal wind is mostly westward, and the seasonal dependence is small. For the nighttime, *Fejer et al.* [2002] revealed from ground-based FPI observations at Millstone Hill that the disturbance zonal wind is also largely independent of season and solar flux level. Their results showed that the westward disturbance wind is much larger during more active periods. All these features can also be found in our CHAMP observations, as shown in Figure 2. In their consecutive study, *Emmert et al.* [2004] have taken all 24 h from WINDII for analyzing the disturbance winds. They found that peak westward disturbance winds occur around 1800 MLT at 60° MLAT and at later local times toward lower latitudes; at 20° MLAT the peak occurs near 0300 MLT (see their Figure 1). When compared to the diurnal variations of the zonal wind as shown in our Figures 4–6, the peak values of our westward disturbance wind appear at almost the same local times as those reported by *Emmert et al.* [2004] for the different latitude regions. There is one interesting feature worth mentioning: the disturbance zonal wind reaches its peak value in the subauroral regions at earlier local times during more active periods. The same feature has also been deduced from WINDII observations, as shown in Figure 1 of *Emmert et al.* [2004]. We come back to this issue further down.

The appearance of the peak westward perturbations shifts to later local times when observed at lower latitudes. This implies that the disturbance wind propagates from high to low latitudes. During magnetically active periods the energy input from the solar wind into the upper atmosphere is most efficiently coupled into the high-latitude ionosphere-thermosphere system. The input energy subsequently causes the high-latitude heating and an enhanced plasma drift, which will further affect the global wind circulation [*Richmond et al.*, 2003b]. *Emmert et al.* [2004] also suggested the heating-induced pressure gradients will generate large equatorward disturbance winds at high latitudes near 0300 MLT, which are further deflected westward due to the Coriolis force. The largest westward perturbation wind appears in the dusk sector, with peak values that shift from 70° at 1800 MLT to 45° at midnight. The authors suggest that this feature is associated with enhanced plasma convection at subauroral regions during disturbed times (see their Figure 4).

In fact, *Wang and Lühr* [2011] already reported that the convection electric field plays a dominant role in association with the occurrence of subauroral polarization streams (SAPS), which are referring to rapid westward (sunward) plasma flows located equatorward of the auroral oval predominantly in the dusk and premidnight sector (1600–2400 MLT) [*Foster and Burke*, 2002]. Region 2 (R2) field-aligned currents in the premidnight sector flow into the ionosphere and close via Pedersen currents through the upward region 1 (R1) currents, located poleward. When Pedersen currents flow in the low-conductivity subauroral region after a poleward leap of the aurora, a large poleward electric field is needed to maintain the current continuity in the ionosphere. In turn it produces relatively fast westward ion drifts [*Anderson et al.*, 2001; *Wang et al.*, 2010]. These fast ion jets drive a westward wind of >200 m/s on average at the latitude where the SAPS peaks [e.g., *Wang et al.*, 2012a]. During less active periods the substorm activity does not expand so far to the evening sector, and consequently, SAPS appear at later local times. We regard this as the reason for the later peak in disturbance wind as observed in Figure 4 for moderate activity.

With SAPS incorporated into the Thermosphere Ionosphere Electrodynamics General Circulation Model (TIEGCM) simulation, *Wang et al.* [2012] showed that SAPS can cause an increase in global thermospheric temperature, and the strong westward ion drift in the SAPS channel imposes a large ion drag effect on the neutrals in the subauroral region. This can be confirmed when comparing the disturbance zonal wind (see our Figure 2b, for active magnetic periods in the Northern Hemisphere) with the SAPS-induced zonal wind (see their Figure 7c). An enhanced westward wind is predicted at 70°N in the afternoon and at 50°N around midnight. The elevated neutral temperature will increase the pressure gradient at high latitudes and further

produces an enhanced equatorward meridional wind, which turns westward at middle and low latitudes under the Coriolis force. Observational evidence for that has also been provided by *Wang et al.* [2012a]. They confirmed that both SAPS and westward zonal wind peak at almost the same latitude. By considering the local ion density, a linear relationship between SAPS ion fluxes and zonal wind is derived for both hemispheres, and the proportionality factor is practically independent of geomagnetic activity.

As the SAPS get stronger with enhanced magnetic activity, it is difficult to fully separate the storm-induced disturbance winds at postmidnight from the effect of SAPS in the evening sector. In any case, SAPS can be considered as the prime drivers for the westward zonal disturbance wind at subauroral latitudes.

4.2. Temporal Evolution of the Disturbance Zonal Wind

In section 3.2 we described a superposed epoch analysis applied to CHAMP wind observations. It is the first time that disturbance winds are analyzed in this way. As shown in Figure 8, the temporal evolution of the disturbance zonal wind after a step-like solar wind input is highly dependent on latitude and MLT. At subauroral regions the disturbance zonal wind is found to be most prominent in the afternoon sector, with the peak response value appearing at 1.5 h after the key time. This is consistent with the intensity evolution of SAPS [*Wang et al.*, 2012b], while for the middle and low latitudes, the disturbance zonal wind is most prominent in the postmidnight sector, with peak values appearing at 3–4.5 h after the key time. The time difference between peak effects at 60° MLAT and the equator amounts to about 3 h, which corresponds to a propagation speed of 610 m/s. This velocity is consistent with the average speed (about 650 m/s) of a traveling atmospheric disturbance (TAD), as reported by *Ritter et al.* [2010]. A Similar velocity has been reported by *Fujiwara et al.* [1996] from model simulations. They found that the horizontal propagation speed of substorm-related atmospheric waves is close to the speed of sound (roughly 440 m/s at about 150 km altitude and 670 m/s at about 260 km altitude). With our superposed epoch analysis we can clearly separate, in particular at low latitudes, the effects of prompt penetration electric field from the disturbance wind effect, which comes several hours later. Quite obvious is also the opposite direction of the prompt penetration effect on the dayside (westward, 1200–1800 MLT) and nightside (eastward, 0000–0600 MLT).

The large-scale atmospheric gravity waves [*Richmond*, 1979a; *Cole and Hickey*, 1981], or TAD [*Prölss and Očko*, 2000], or the meridional circulation [*Richmond*, 1979b; *Burns et al.*, 1989] is considered to transport the storm or substorm-related energy that is injected into the high latitude down to low latitudes. The enhanced meridional wind will later be deflected westward by the Coriolis force. At equatorial regions these disturbance winds will further affect the global ionospheric dynamo. Because of the inertia of the neutral air, a few hours are required to set up the disturbance winds. Once they are set up, they can persist for several hours [*Richmond et al.*, 2003b]. Thus, low-latitude electric field disturbances associated with disturbance winds tend to be more persistent than those associated with changes from the prompt penetration electric field. By model simulation *Maruyama et al.* [2005] reported that the prompt penetration electric field is dominant for ionospheric currents during daytime and at the early stage of a storm, while the disturbance dynamo effects become important at nighttime. This is consistent with our CHAMP observations that at equatorial regions the westward disturbance wind is most prominent during the postmidnight hours. During daytime the *F* region ionosphere is strongly coupled to the *E* region dynamo process, while at nighttime the *F* region dynamo plays a dominant role.

Finally, we would like to note that the disturbance wind caused by magnetic activity is just one contributor to the large variability of *F* region zonal winds. Its importance should thus not be overestimated. For example, at subauroral latitudes we find almost no disturbance winds in the time sector 0000–0900 MLT (see Figure 4). In spite of that the wind variability is largest during those hours (see Figure 3). This clearly shows the influence of other effects like tides [e.g., *Xiong et al.*, 2015] or longitude dependences [e.g., *Häusler et al.*, 2007] in combination with seasonal dependences. This relation becomes even more obvious when considering the small fraction of hours with $Kp > 4$ contributing to the result of Figure 3. Due to the many other wind effects, it is difficult to identify the ionospheric currents caused by the disturbance dynamo. It would be interesting to study in which regions the disturbance winds act as a generator or a load.

5. Summary

Based on 5 years data (from 2001 to 2005) of CHAMP zonal wind observations, we investigate the global features and the temporal evolution of the storm time driven disturbance winds in the topside ionosphere.

These winds can be considered as an important element for coupling high- and low-latitude activity. Our main results are summarized as follows:

1. The disturbance zonal wind is mainly directed westward. It gets stronger with larger magnetic activity and toward higher latitudes.
2. During disturbed periods the westward zonal wind at subauroral region is strongly enhanced within the MLT sector from afternoon to midnight, which we related to coupling with SAPS activity. At low and middle latitudes the disturbance zonal wind is practically independent of season.
3. During more active periods ($Kp > 4$), the peak values of the disturbance zonal wind appear at different local times for different latitude bands. That is around 1800 MLT at subauroal regions, with peak values of about 200 m/; around 2300 MLT at middle latitudes, with peak values of about 80 m/s; and around 0300 MLT at low latitudes, with peak values of about 50 m/s. This shift in MLT of the peak wind speed toward lower latitudes could be considered as a result of the propagation from high to low latitudes.
4. We applied for the first time a superposed epoch analysis for studying the response to a step-like solar wind input. It shows that the disturbance wind effect is first observed at auroral latitudes, and it needs 3–4 h to reach the equator. This delay time is consistent with the speed of TAD. At the same time clear signature of the prompt penetration effect is visible, in particular at low latitudes. The latter effect causes oppositely directed wind deflections on the dayside and nightside.

In a subsequent study we plan to investigate the effect of the disturbance winds on ionospheric currents. From related observations we may deduce dynamo effects of the disturbance winds.

Acknowledgments

The CHAMP mission was sponsored by the Space Agency of the German Aerospace Center (DLR) through funds of the Federal Ministry of Economics and Technology. The CHAMP thermospheric zonal wind data are available at the website of air density models derived from multisatellite drag observations (http://thermosphere.tudelft.nl/acceldrag/data.php). The wind data type we used is CH_PN_R03. The work of Chao Xiong is supported by the Alexander von Humboldt Foundation through a Research Fellowship for Postdoctoral Researchers.

Larry Kepko thanks Miguel Larsen and Arthur Richmond for their assistance in evaluating this paper.

References

Anderson, P. C., D. L. Carpenter, K. Tsuruda, T. Mukai, and F. J. Rich (2001), Multisatellite observations of rapid subauroral ion drifts (SAID), *J. Geophys. Res.*, *106*, 29,585–29,600, doi:10.1029/2001JA000128.

Aruliah, A. L., A. D. Farmer, D. Rees, and U. Brandstrøm (1996), The seasonal behaviour of high-latitude thermospheric winds and ion velocities observed over one solar cycle, *J. Geophys. Res.*, *101*, 15,701–15,711, doi:10.1029/96JA00360.

Babcock, R. R., and J. V. Evans (1979), Effects of geomagnetic disturbances on neutral winds and temperatures in the thermosphere observed over Millstone Hill, *J. Geophys. Res.*, *84*(A9), 5349–5354, doi:10.1029/JA084iA09p05349.

Blanc, M., and A. D. Richmond (1980), The ionospheric disturbance dynamo, *J. Geophys. Res.*, *85*, 1669–1686, doi:10.1029/JA085iA04p01669.

Buonsanto, M. J., and O. G. Witasse (1999), An updated climatology of thermospheric winds and *F* region ion drifts over Millstone Hill, *J. Geophys. Res.*, *104*, 24,675–24,687, doi:10.1029/1999JA900345.

Burke, W. J., C. Y. Huang, F. A. Marcos, and J. O. Wise (2007), Interplanetary control of thermospheric densities during large magnetic storms, *J. Atmos. Sol. Terr. Phys.*, *69*, 279–287.

Burns, A. G., T. L. Killeen, G. Crowley, B. A. Emery, and R. G. Robie (1989), On the mechanisms responsible for high-latitude thermospheric composition variations during the recovery phase of a geomagnetic storm, *J. Geophys. Res.*, *94*(A12), 16,961–16,968, doi:10.1029/JA094iA12p16961.

Codrescu, M. V., T. J. Fuller-Rowell, V. Munteanu, C. F. Minter, and G. H. Millward (2008), Validation of the coupled thermosphere ionosphere plasmasphere electrodynamics model: CTIPe-Mass Spectrometer Incoherent Scatter temperature comparison, *Space Weather*, *6*, S09005, doi:10.1029/2007SW000364.

Cole, K. D., and M. P. Hickey (1981), Energy transfer by gravity wave dissipation, *Adv. Space Res.*, *1*, 65–75.

Doornbos, E., J. Ijssel, H. Lühr, M. Förster, and G. Koppenwallner (2010), Neutral density and crosswind determination from arbitrarily oriented multiaxis accelerometers on satellites, *J. Spacraft Rockets*, *47*(4), 580–589, doi:10.2514/1.48114.

Drob, D. P., et al. (2008), An empirical model of the Earth's horizontal wind fields: HWM07, *J. Geophys. Res.*, *113*, A12304, doi:10.1029/2008JA013668.

Emmert, J. T., B. G. Fejer, C. G. Fesen, G. G. Shepherd, and B. H. Solheim (2001), Climatology of middle- and low-latitude daytime *F* region disturbance neutral winds measured by Wind Imaging Interferometer (WINDII), *J. Geophys. Res.*, *106*(A11), 24701–24712, doi:10.1029/2000JA000372.

Emmert, J. T., B. G. Fejer, G. G. Shepherd, and B. H. Solheim (2004), Average nighttime *F* region disturbance neutral winds measured by UARS WINDII: Initial results, *Geophys. Res. Lett.*, *31*, L22807, doi:10.1029/2004GL021611.

Emmert, J. T., D. P. Drob, G. G. Shepherd, G. Hernandez, M. J. Jarvis, J. W. Meriwether, R. J. Niciejewski, D. P. Sipler, and C. A. Tepley (2008), DWM07 global empirical model of upper thermospheric storm-induced disturbance winds, *J. Geophys. Res.*, *113*, A11319, doi:10.1029/2008JA013541.

Emmert, J. T., A. D. Richmond, and D. P. Drob (2010), A computationally compact representation of magnetic-apex and quasi-dipole coordinates with smooth base vectors, *J. Geophys. Res.*, *115*, A08322, doi:10.1029/2010JA015326.

Fejer, B. G., J. T. Emmert, G. G. Shepherd, and B. H. Solheim (2000), Average daytime *F* region disturbance neutral winds measured by UARS: Initial results, *Geophys. Res. Lett.*, *27*(13), 1859–1862.

Fejer, B. G., J. T. Emmert, and D. P. Sipler (2002), Climatology and storm time dependence of nighttime thermospheric neutral winds over Millstone Hill, *J. Geophys. Res.*, *107*(A5), SIA 3–1–SIA 3-9, doi:10.1029/2001JA000300.

Foster, J. C., and W. J. Burke (2002), SAPS: A new categorization for sub-auroral electric fields, *EOS Trans. AGU*, *83*, 393–394, doi:10.1029/2002EO000289.

Fujiwara, H., S. Maeda, H. Fukunishi, T. J. Fuller-Rowell, and D. S. Evans (1996), Global variations of therrnospheric winds and temperatures caused by substorm energy injection, *J. Geophys. Res.*, *101*(A1), 225–239, doi:10.1029/95JA01157.

Häusler, K., H. Lühr, S. Rentz, and W. Köhler (2007), A statistical analysis of longitudinal dependences of upper thermospheric zonal winds at dip equator latitudes derived from CHAMP, *J. Atmos. Sol. Terr. Phys.*, *69*, 1419–1430, doi:10.1016/j.jastp.2007.04.004.

Hedin, A. E., et al. (1996), Empirical wind model for the upper, middle and lower atmosphere, *J. Atmos. Sol. Terr. Phys.*, *58*, 1421–1447.

Kan, J. R., and L. C. Lee (1979), Energy coupling function and solar wind-magnetosphere dynamo, *Geophys. Res. Lett.*, *6*, 577–580, doi:10.1029/GL006i007p00577.
Kikuchi, T., H. Lühr, T. Kitamura, O. Saka, and K. Schlegel (1996), Direct penetration of the polar electric field to the equator during a DP 2 event as detected by the auroral and equatorial magnetometer chains and the EISCAT radar, *J. Geophys. Res.*, *101*(A8), 4327–4341, doi:10.1029/96JA01299.
Killeen, T., and R. G. Roble (1988), Thermosphere dynamics: Contributions from the first 5 years of the dynamics explorer program, *Rev. Geophys.*, *26*, 329–367, doi:10.1029/RG026i002p00329.
Killeen, T., et al. (1986), Mean neutral circulation in the winter polar *F*-region, *J. Geophys. Res.*, *91*, 1633–1649, doi:10.1029/JA091iA02p01633.
Liu, H., H. Lühr, S. Watanabe, W. Köhler, V. Henize, and P. Visser (2006), Zonal winds in the equatorial upper thermosphere: Decomposing the solar flux, geomagnetic activity, and seasonal dependencies, *J. Geophys. Res.*, *111*, A07307, doi:10.1029/2005JA011415.
Liu, R., H. Lühr, E. Doornbos, and S.-Y. Ma (2010), Thermospheric mass density variations during geomagnetic storms and a prediction model based on the merging electric field, *Ann. Geophys.*, *28*, 1633–1645, doi:10.5194/angeo-28-1633-2010.
Lühr, H., S. Rentz, P. Ritter, H. Liu, and K. Häusler (2007), Average thermospheric wind patterns over the polar regions, as observed by CHAMP, *Ann. Geophys.*, *25*, 1093–1101, doi:10.5194/angeo-25-1093-2007.
Maruyama, N., A. D. Richmond, T. J. Fuller-Rowell, M. V. Codrescu, S. Sazykin, F. R. Toffoletto, R. W. Spiro, and G. H. Millward (2005), Interaction between direct penetration and disturbance dynamo electric fields in the storm-time equatorial ionosphere, *Geophys. Res. Lett.*, *32*, L17105, doi:10.1029/2005GL023763.
Newell, P. T., T. Sotirelis, K. Liou, C.-I. Meng, and F. J. Rich (2007), A nearly universal solar wind-magnetosphere coupling function inferred from 10 magnetospheric state variables, *J. Geophys. Res.*, *112*, A01206, doi:10.1029/2006JA012015.
Prölss, G. W., and M. Očko (2000), Thermospheric response to a magnetic substorm, *Adv. Space Res.*, *26*(1), 131–135.
Rees, D., T. Fuller-Rowell, and R. W. Smith (1980), Measurements of high latitude thermospheric winds by rocket and ground-based techniques and their interpretation using a three-dimensional time-dependent dynamical model, *Planet. Space Sci.*, *28*, 919–932, doi:10.1016/0032-0633(80)90064-1.
Reigber, C., H. Lühr, and P. Schwintzer (2002), CHAMP mission status, *Adv. Space Res.*, *30*, 129–134.
Richmond, A. D. (1979a), Large-amplitude gravity wave energy production and dissipation in the thermosphere, *J. Geophys. Res.*, *84*(A5), 1880–1890, doi:10.1029/JA084iA05p01880.
Richmond, A. D. (1979b), Thermospheric heating in a magnetic storm: Dynamic transport of energy from high to low latitudes, *J. Geophys. Res.*, *84*(A9), 5259–5266, doi:10.1029/JA084iA09p05259.
Richmond, A. D. (1995), Ionospheric electrodynamics using magnetic apex coordinates, *J. Geomagn. Geoelectr.*, *47*, 191–212, doi:10.1029/92GL00401.
Richmond, A. D., E. C. Ridley, and R. G. Roble (1992), A thermosphere/ionosphere general circulation model with coupled electrodynamics, *Geophys. Res. Lett.*, *19*(6), 601–604, doi:10.1029/92GL00401.
Richmond, A. D., C. Lathuillère, and S. Vennerstroem (2003a), Winds in the high-latitude lower thermosphere: Dependence on the interplanetary magnetic field, *J. Geophys. Res.*, *108*(A2), 1066, doi:10.1029/2002JA009493.
Richmond, A. D., C. Peymirat, and R. G. Roble (2003b), Long-lasting disturbances in the equatorial ionospheric electric field simulated with a coupled magnetosphere-ionosphere-thermosphere model, *J. Geophys. Res.*, *108*(A3), 1118, doi:10.1029/2002JA009758.
Ridley, A. J., Y. Deng, and G. Tóth (2006), The global ionosphere–thermosphere model, *J. Atmos. Sol. Terr. Phys.*, *68*, 839–864.
Ritter, P., H. Lühr, and E. Doornbos (2010), Substorm-related thermospheric density and wind disturbances derived from CHAMP observations, *Ann. Geophys.*, *28*, 1207–1220, doi:10.5194/angeo-28-1207-2010.
Sipler, D. P., B. B. Luokkala, and M. A. Biondi (1982), Fabry-Perot determinations of mid-latitude *F*-region neutral winds and temperatures from 1975 to 1979, *Planet. Space Sci.*, *20*, 1025–1032, doi:10.1016/0032-0633(82)90152-0.
Sipler, D. P., M. E. Hagan, M. E. Zipf, and M. A. Biondi (1991), Combined optical and radar wind measurements in the *F* region over Millstone Hill, *J. Geophys. Res.*, *96*(A12), 21,255–21,262, doi:10.1029/91JA02371.
Thayer, J. P., T. L. Killeen, F. G. McCormac, C. R. Tschan, J.-J. Ponthieu, and N. W. Spencer (1987), Thermospheric neutral wind signatures dependent on the east-west component of the interplanetary magnetic field for Northern and Southern Hemispheres, *Ann Geophys.*, *5*, 363–368.
VanHelleputte, T., E. Doornbos, and P. Visser (2009), CHAMP and GRACE accelerometer calibration by GPS-based orbit determination, *Adv. Space Res.*, *43*(12), 1890–1896.
Wang, H., and H. Lühr (2011), The efficiency of mechanisms driving Subauroral Polarization Streams (SAPS), *Ann Geophys.*, *29*, 1277–1286, doi:10.5194/angeo-29-1277-2011.
Wang, H., H. Lühr, and A. J. Ridley (2010), Plasma convection jets near the poleward boundary of the nightside auroral oval and their relation to Pedersen conductivity gradients, *Ann Geophys.*, *28*, 969–976, doi:10.5194/angeo-28-969-2010.
Wang, H., H. Lühr, and S. Y. Ma (2012a), The relation between subauroral polarization streams, westward ion fluxes, and zonal wind: Seasonal and hemispheric variations, *J. Geophys. Res.*, *28*, 969–976, doi:10.1029/2011JA017378.
Wang, H., H. Lühr, P. Ritter, and G. Kervalishvili (2012b), Temporal and spatial effects of subauroral polarization streams on the thermospheric dynamics, *J. Geophys. Res.*, *117*, A11307, doi:10.1029/2012JA018067.
Wang, W., E. R. Talaat, A. G. Burns, B. Emery, S. Hsieh, J. Lei, and J. Xu (2012), Thermosphere and ionosphere response to subauroral polarization streams (SAPS): Model simulations, *J. Geophys. Res.*, *117*, A07301, doi:10.1029/2012JA017656.
Werner, S., and G. W. Prölss (1997), The position of the ionospheric trough as a function of local time and magnetic activity, *Adv. Space Res.*, *20*(9), 1717–1722.
Witasse, O., J. Lilensten, C. Lathuillere, and B. Pibraret (1998), Meridional thermospheric neutral wind at high latitude over a full solar cycle, *Ann. Geophys.*, *16*, 1400–1409, doi:10.5194/angeo-32-623-2014.
Xiong, C., and H. Lühr (2014), An empirical model of the auroral oval derived from CHAMP field-aligned current signatures—Part 2, *Ann. Geophys.*, *32*, 623–631, doi:10.5194/angeo-32-623-2014.
Xiong, C., H. Lühr, H. Wang, and M. G. Johnsen (2014), Determining the boundaries of the auroral oval from CHAMP field aligned current signatures—Part 1, *Ann. Geophys.*, *32*, 609–622, doi:10.5194/angeo-32-609-2014.
Xiong, C., Y.-L. Zhou, H. Lühr, and S.-Y. Ma (2015), Tidal signatures of the thermospheric mass density and zonal wind at midlatitude: CHAMP and GRACE observations, *Ann. Geophys.*, *33*, 185–196, doi:10.5194/angeo-33-185-2015.